Eur Biophys J (1991) 19:169–181

European Biophysics Journal

Distributions of oxygen, nutrient, and metabolic waste concentrations in multicellular spheroids and their dependence on spheroid parameters

K. Groebe and W. Mueller-Klieser

Institut für Physiologie und Pathophysiologie, Universität Mainz, Saarstrasse 21, W-6500 Mainz, Federal Republic of Germany

Received February 19, 1990/Accepted in revised form September 21, 1990

Abstract. The distribution of oxygen, nutrients and metabolic wastes in multicellular tumor spheroids and its dependence on the parameters characterizing the spheroid (i.e., spheroid geometry, diffusivity, and consumption/production rates of biological substances) have been investigated by a theoretical analysis: *1.* Parameter dependence is qualitatively demonstrated and visualized. *2.* Reduction of the number of variables by specific coordinate transformations made it possible to generate nomograms from which concentration distributions for any choice of parameter values may easily be obtained. In particular, these nomograms may also be used for estimating concentration profiles of metabolic waste products, e.g. of lactate, which are expected to accumulate in the tumor spheroids. *3.* An additional set of nomograms is given which is more convenient for determining time courses of these concentrations during spheroid growth. *4.* A quantitative sensitivity analysis of parameter dependencies is performed to identify those parameters upon which a concentration of interest depends most critically in a given experimental situation.

Key words: Multicellular tumor spheroids – Concentration distribution – Parameter dependence – Mathematical model – Nomogram – Metabolite diffusion – Metabolite consumption/production

Introduction

Multicellular tumor spheroids have been widely used in experimental cancer research as model systems of tumor microregions (for reviews see: Mueller-Klieser 1987; Sutherland 1988; Carlsson and Nederman 1989). One major focus of interest is the simulation of tumor therapy in vivo. For example, studies on the radiosensitivity of cancer cells cultured as spherical aggregates as well as investigations on the susceptibility of spheroid cells to radiosensitizing or antiproliferative drugs have been performed extensively by numerous investigators for the past decade.

There is evidence from many of these studies that microenvironmental factors, such as O_2 and nutrient supply as well as accumulation of metabolic wastes in tumor microregions may greatly influence metabolism and, hence, the resistance of cancer cells to therapy which is a general feature of three-dimensional tumor cell growth both in vitro and in vivo. Thus, quantitative knowledge of the tumor micromilieu is needed to better understand the mechanisms involved in the development of resistance to treatment. In tumor spheroids it is not possible to characterize this micromilieu only by substance concentrations in the medium as the exchange of nutrients and metabolic waste products takes place by diffusion and hence their concentrations change with depth into the spheroid. Rather, concentration distributions within the spheroid have to be considered in evaluating the interactions between metabolically active substances and reaction to treatment.

Only a few investigations have been published to date concerning direct measurements of the distribution of O_2, H^+ ions or nutrients in multicellular tumor spheroids (for reviews see: Acker et al. 1984; Mueller-Klieser 1987; Sutherland 1988). Theoretical approaches have been made to determining the distribution of substances of interest within spheroids such as O_2 (Mueller-Klieser and Sutherland 1982a, b; Bush et al. 1982; Carlsson and Acker 1985; Freyer and Sutherland 1986) or glucose (Mueller-Klieser and Sutherland 1982a, b; Freyer and Sutherland 1983; Freyer and Sutherland 1985).

Diffusion theory allows one to predict the distributions of O_2, nutrients and metabolic waste products in multicellular tumor spheroids on a very general basis. Assuming spherical symmetry and constant diffusivity and substance consumption/production rate throughout the viable rim of a spheroid, there are only 7 parameters on which concentration profiles depend: The radii of the spheroid, s; of the central necrosis, n; and of a layer of unstirred medium (diffusion depleted zone) surrounding

Offprint requests to: W. Mueller-Klieser

the spheroid, g; the diffusivities in the surrounding medium, D_M; and within the spheroid, D_S; the substance consumption/production rate, Q; and the substance concentration in the free medium, C_B. In the present study the dependencies of concentration profiles on these parameters are assessed and nomograms are given which allow one to determine the concentration at any location within the spheroid for any combination of these parameters with only a few simple calculations. In particular, the paper proceeds through the following steps:

1. The dependencies of concentration profiles (or, more specifically, partial pressure profiles) on each one of the above parameters are visualized for the special case of a sample spheroid and the sample substance oxygen.

2. The above mentioned nomograms are given and their use is illustrated.

3. In a number of situations there is particular interest in concentration changes during spheroid growth. Therefore, an additional set of nomograms is introduced which allow one to assess these changes more conveniently.

4. A sensitivity analysis is performed which may be used to identify those parameters on which concentration profiles depend most critically.

Methods

Multicellular tumor spheroids growing in a spinner flask typically exhibit a layer of unstirred medium surrounding the spheroid, a spherical rim of viable tumor cells, and a central concentric necrotic region. Substance diffusivity and consumption/production rate are assumed to be constant throughout the viable rim. The steady state diffusion equation for this arrangement has been solved previously (Mueller-Klieser 1984a; see also Eqs. (A3), Appendix).

Whenever gaseous solutes are considered, the partial pressure P is used instead of the concentration C. Accordingly, the diffusion coefficients in medium and spheroids, D_M and D_S, have to be replaced by the respective conductivities (also referred to as "Krogh's diffusion coefficients") K_M and K_S that are defined as diffusion coefficient times solubility of the gas.

The solution of the differential equation of diffusion depends on a number of parameters. These parameters along with the abbreviations used are listed below:

D_M, D_S	diffusion coefficients of dissolved solid or liquid substrates/wastes in the medium and in the spheroid, respectively
K_M, K_S	conductivities of dissolved gaseous substrates in the medium and in the spheroid, respectively
Q	volume-related substrate consumption/production rate (negative in the case of production)
n, s, g	radii of central necrosis, spheroid, and diffusion-depleted zone, respectively
r	radial position
$C(r)$	substance concentration at radial position r
C_B	substance concentration at the interface between stirred medium and diffusion-depleted zone
r', n', g'	dimensionless radial coordinate, dimensionless radii of central necrosis and of diffusion-depleted zone, respectively
C'	dimensionless substance concentration

In step 1 (see Introduction), families of Po_2-profiles are plotted for variations in one particular parameter. The mathematics required for steps 2.–4. are detailed in the Appendix: In order to yield a form which is suitable for nomogram representation, dimensionless coordinates are introduced, and (A3) are transformed accordingly. For step 4. the derivatives of (A3) with respect to the above parameters are required and these may be calculated in a straightforward fashion. They are compiled in Table 1.

Results and specific discussion

1. Dependence of concentration distributions on parameter values

In this section, parameter dependencies of concentration profiles $C(r)$ are qualitatively demonstrated and visualized. To this end, the special case of oxygen as a substrate and of a spheroid – denoted below as "sample spheroid" – with a diameter of 500 μm, an unstirred layer thickness of 50 μm, and a diameter of the central necrosis of 100 μm is considered. Based on data from previous studies (Mueller-Klieser 1984b), we assume the oxygen consumption rate to be $4 \cdot 10^{-4}$ ml O_2/(cm^3 tissue · s), the diffusion conductivities outside the spheroid, K_M, to be $1.02 \cdot 10^{-9}$ ml O_2/(cm · mmHg · s) and inside the spheroid, K_S, to be $0.51 \cdot 10^{-9}$ ml O_2/(cm · mmHg · s). This set of data describing our "standard spheroid" was chosen as a representative example of values recorded in multicellular tumor spheroids of EMT6/Ro-cells in previous investigations (Mueller-Klieser et al. 1986). For gaseous solutes such as oxygen, it is more convenient to replace their concentration C by their partial pressure P which is C divided by the solubility of the gas.

In Fig. 1 a–e various sets of Po_2 profiles are plotted, each one being parameterized by an individual one of the above parameters. Po_2 outside the unstirred layer is set to 0, i.e., Po_2 drops between free medium and spheroid are displayed. In each of Fig. 1 a–e, the bold line denotes the profile pertinent to the sample spheroid specified above. The different zones which the "spheroid system" is made up of are easily distinguished in the profiles: The horizontal portion next to the spheroid center corresponds to the central necrosis (not always present), the subsequent steep portion is composed of the Po_2 drops in the viable rim and in the unstirred layer. Most of the profiles exhibit a clear cut break near the outer edge of this steep portion which marks the position of the interface between the two regions (see arrows in Fig. 1 a–e). In the free medium outside of the unstirred layer profiles are constant again.

Except for very large necroses, changes in necrosis diameter hardly affect $C(r)$ within the unstirred layer and the viable rim (Fig. 1 a). In plotting the profiles for varying spheroid radii (Fig. 1 b), the viable rim thickness is kept

Table 1. "Sensitivities" governing the propagation of dimensionless errors $\Delta p_i/p_i$ in the i-th parameter of the parameter vector p into the calculated substrate concentration for the respective zones, given as a function of the actual parameter values. In the case of gaseous solutes, C, C_B, D_M, and D_S have to be replaced by P, P_B, K_M, and K_S, respectively

Parameter p_i	General terms	Medium $r>g$	Diffusion depleted zone $(s<r\leq g)$	Viable rim $(n<r\leq s)$	Necrosis $(r\leq n)$
r	$\frac{\partial C}{\partial r}r$	0	$\frac{Q}{3D_M r}(s^3-n^3)$	$\frac{Q}{3D_S}\left(r^2-\frac{n^3}{r}\right)$	0
n	$\frac{\partial C}{\partial n}n$	0	$\frac{Q\,n^3}{D_M}\left(\frac{1}{r}-\frac{1}{g}\right)$	$\frac{Q\,n^3}{D_M}\left(\frac{1}{s}-\frac{1}{g}\right)+\frac{Q\,n^3}{D_S}\left(\frac{1}{r}-\frac{1}{s}\right)$	$\frac{Q\,n^3}{D_M}\left(\frac{1}{s}-\frac{1}{g}\right)+\frac{Q\,n^3}{D_S}\left(\frac{1}{n}-\frac{1}{s}\right)$
s	$\frac{\partial C}{\partial s}s$	0	$-\frac{Q\,s^3}{D_M}\left(\frac{1}{r}-\frac{1}{g}\right)$	$\frac{Q}{3D_M}\left(\frac{3s^3}{g}-2s^2-\frac{n^3}{s}\right)+\frac{Q}{3D_S}\left(\frac{n^3}{s}-s^2\right)$	
g	$\frac{\partial C}{\partial g}g$	0	$-\frac{Q}{3D_M g}(s^3-n^3)$		
Q	$\frac{\partial C}{\partial Q}Q$	0	$C-C_B$ (for C see Eqs. (A3))		
D_M	$\frac{\partial C}{\partial D_M}D_M$	0	$\frac{Q}{3D_M}(s^3-n^3)\left(\frac{1}{r}-\frac{1}{g}\right)$	$\frac{Q}{3D_M}(s^3-n^3)\left(\frac{1}{s}-\frac{1}{g}\right)$	
D_S	$\frac{\partial C}{\partial D_S}D_S$	0	0	$\frac{Q}{6D_S}\left(s^2-r^2+\frac{2n^3}{s}-\frac{2n^3}{r}\right)$	$\frac{Q}{6D_S}\left(s^2+\frac{2n^3}{s}-3n^2\right)$
C_B	$\frac{\partial C}{\partial C_B}C_B$	C_B	C_B	C_B	C_B

constant as this is typical for "physiological" growth of various spheroid types (see e.g.: Conger and Ziskin 1983; Freyer and Sutherland 1986; Carlsson and Acker 1988). Thus, the large differences in Po_2 drops are only due to changes in the curvature of the oxygen consuming layer of the same thickness. Changes in the unstirred layer thickness do not affect intra-spheroidal portions of Po_2 profiles except for shifting their offset Po_2 value (Fig. 1 c). Similarly, the shapes of the profiles inside the spheroid are not changed by variations in D_M (similar to Fig. 1 c). Vice versa, $C(r)$ inside the unstirred layer does not depend upon variations in D_S (Fig. 1 d). Since intra-spheroidal profiles depend on the ratio of Q/D_S, the set of intra-spheroidal profiles resulting from variations in D_S (Fig. 1 d) is the same as that found for changes in the consumption rate Q (Fig. 1 e). In the latter case, however, Po_2 drops across the unstirred layer are affected also.

As shown in Appendix, Eq. (A4), the ratio of the concentration gradients dC/dr above and below the spheroid surface (break in the steep portions of the profiles) is equal to the ratio of the diffusion coefficients in spheroid and medium D_S/D_M. For gaseous solutes, this is the ratio of Krogh's diffusion coefficients K_S/K_M. Consequently, it is possible to calculate D_S, if D_M and the ratio

$$\frac{dC/dr(s^+)}{dC/dr(s^-)}$$

(s^+, s^-: upper and lower limits) have been determined from experiments.

Variations in the substrate consumption rate Q as well as variations in the spheroid geometry may both alter the overall amount of substrate consumed. Consequently, such variations may change the whole profile inside and outside the spheroid (Fig. 1 a, b, e). Note that the changes of the profile inside the spheroid caused by a variation of Q are the same as changes caused by an inversely proportional variation of D_S. This may easily be seen from (A3), since inside the viable rim the dependence of $C(r)$ on D_S and Q is actually a dependence on Q/D_S. Moreover, in the unstirred layer, $C(r)$ only depends on spheroid geometry, D_M, and Q, not however, on D_S (Fig. 1 d). Thus, from measurements of concentration distributions inside the diffusion depleted zone the substrate consumption rate Q may be determined without knowledge of D_S. This is the basis of the analytical method given by Mueller-Klieser (1984 a).

2. Diagrams of dimensionless concentration distributions and their use

The mathematics required to transform (A3) to a form suitable for nomogram representation is dealt with in the Appendix. In the nomograms of Fig. 2 a–g dimensionless coordinates are applied. For a spheroid of radius s, the radial coordinate r corresponds to the dimensionless radial coordinate r' according to

$$r'=\frac{r}{s} \tag{1}$$

Note that $r'=0$ corresponds to the spheroid center, $r'=1$ corresponds to the spheroid surface and values greater

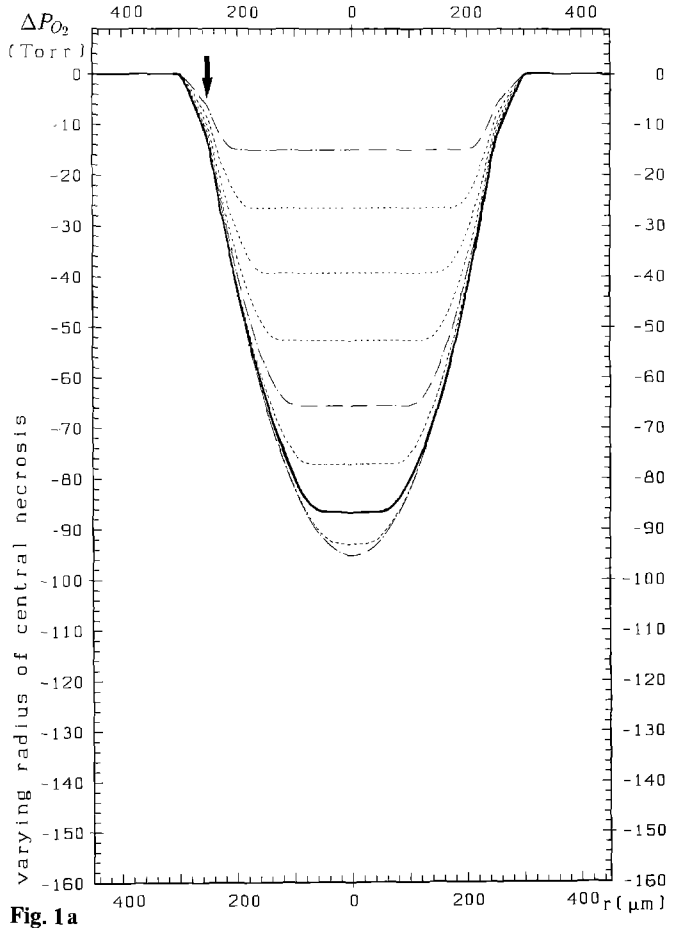

Fig. 1a

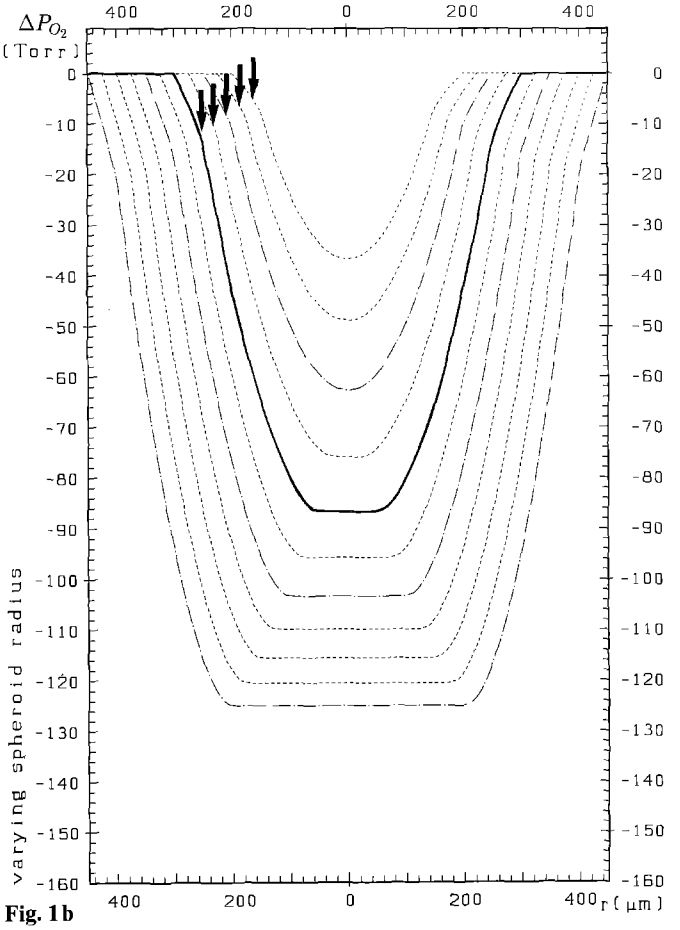

Fig. 1b

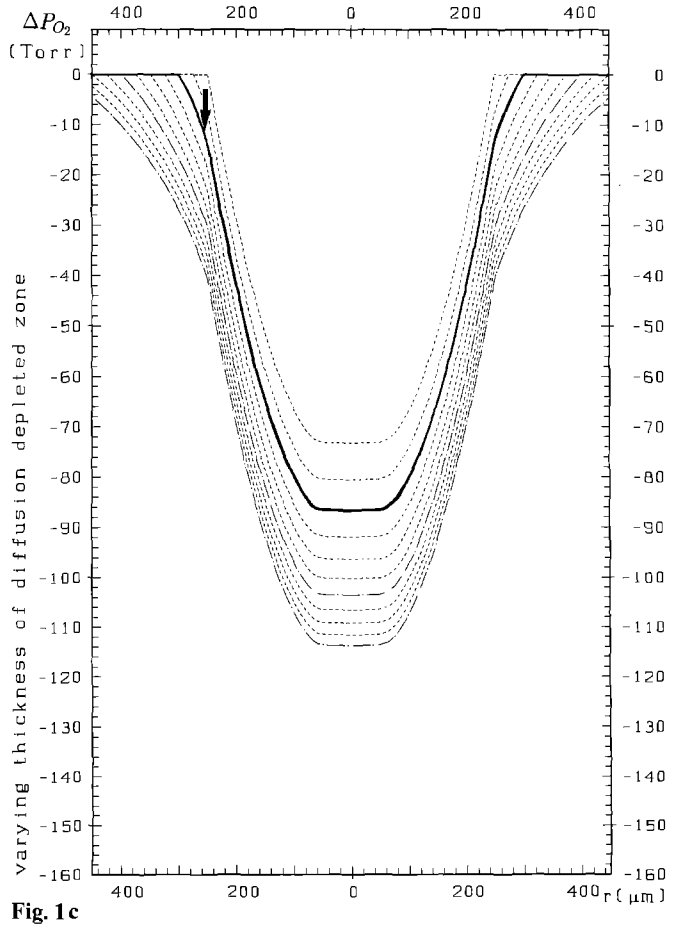

Fig. 1c

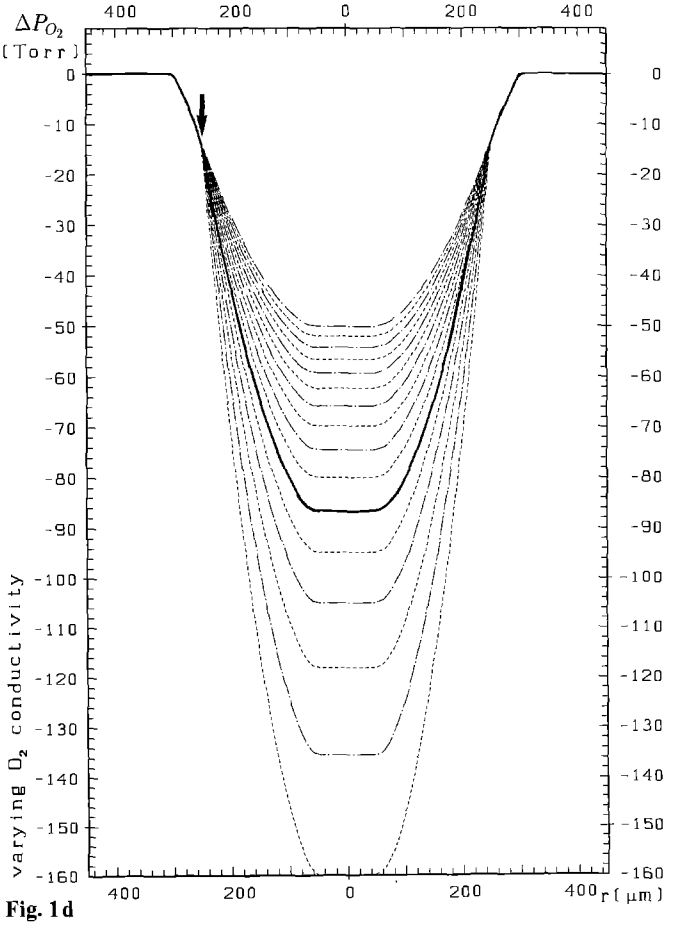

Fig. 1d

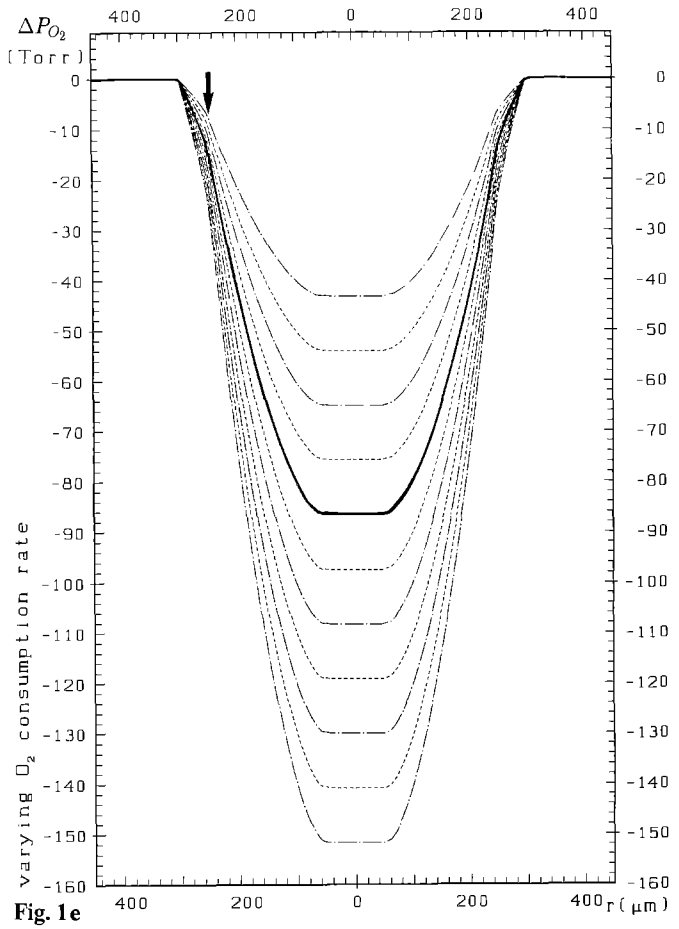

Fig. 1e

Fig. 1a–e. Distributions of differences ΔPo_2 between stirred medium Po_2 and local Po_2 inside diffusion depleted zone and spheroid for varying values of **a** radius of central necrosis (increment: 25 μm); **b** spheroid radius (increment 25 μm); **c** diffusion depleted zone thickness (increment 25 μm); **d** spheroid conductivity K_S (increment: 0.05 units of K_S/K_M); **e** O_2 consumption rate Q (increment: $0.5 \cdot 10^{-4}$ ml O_2/(cm^3 tissue · s)). Bold lines depict Po_2 profiles inside a "sample spheroid" ($s=250$ μm; viable rim thickness: $d=s-n=200$ μm; thickness of diffusion-depleted zone: $g-s=50$ μm; $Q=4 \cdot 10^{-4}$ ml O_2/(cm^3 tissue · s); $K_M=1.02 \cdot 10^{-9}$ ml O_2/(cm · mmHg · s); $K_S=0.51 \cdot 10^{-9}$ ml O_2/(cm · mmHg · s)). Arrows indicate the positions of interfaces between viable rims and diffusion-depleted zones

than 1 represent locations within the diffusion depleted zone. In particular, the dimensionless radii of the unstirred layer and of the central necrosis are $g'=g/s$ and $n'=n/s$, respectively, where g and n are their dimensional radii.

The thickness of the unstirred layer primarily depends on the rate of stirring of the medium surrounding the spheroid and has been reported to be in the range 90–110 μm in chambers for Po_2 measurements in spheroids (Mueller-Klieser et al. 1986). The respective thickness in spinner flasks that are commonly used for spheroid growth is about 60–80 μm (Casciari 1989; see Table 4 in Appendix).

The nomogram to apply in a given situation and the curve to read from are chosen as follows. The choice is based on the radii of the central necrosis and of the spheroid (which can be measured in a histological section) and on the substance diffusivities in medium and spheroid (which may be obtained from the literature, e.g., Mueller-Klieser 1984a; for various gases, ratios of conductivities across the interfaces of several liquid/tissue systems have been compiled, e.g. by Kawashiro et al. 1975). Each of Fig. 2a–g relates to a different dimensionless radius n' of the central necrosis that may be easily identified as the abscissal value below which the concentration profiles are constant. In each nomogram, the displayed set of curves is parameterized by the ratio of the diffusion coefficient inside the spheroid over the diffusion coefficient outside the spheroid, D_S/D_M, or the ratio of the corresponding diffusion conductivities (Krogh's diffusion coefficients) K_S/K_M. D_S/D_M was chosen instead of the more straightforward ratio D_M/D_S because the former one is more commonly used in the literature. Note that the profile within the diffusion depleted zone does not depend upon this ratio.

After the nomogram and the curve in the nomogram appropriate for the spheroid considered have been chosen, one calculates the dimensionless radial coordinates r' and g' (abscissae of the nomogram) according to $r'=r/s$ and $g'=g/s$ where r is the dimensional radial coordinate at which the substance concentration is to be determined, g is the radius of the diffusion-depleted zone, and s is the spheroid radius.

The ordinate in Fig. 2a–g is the dimensionless concentration C'. Dimensionless concentrations are read from the appropriate curve at radial positions r' and g' yielding $C'(r')$ and $C'(g')$, respectively. These numbers may be converted to a dimensional concentration $C(r)$ by

$$C(r)=C_B-\frac{Q}{D_M}\,s^2(C'(g')-C'(r')) \qquad (2)$$

where

C_B	concentration in bulk medium
Q	volume-related substrate consumption/production rate (negative in case of production)
D_M	diffusion coefficient in medium
s	spheroid radius
$C'(g')$	dimensionless concentration at the edge of the diffusion-depleted zone $g'=g/s$
$C'(r')$	dimensionless concentration at the dimensionless radius $r'=r/s$

In the case of gaseous solutes we have, by analogy, for the partial pressure $P(r)$

$$P(r)=P_B-\frac{Q}{K_M}\,s^2(C'(g')-C'(r')) \qquad (3)$$

where additionally

P_B	partial pressure in bulk medium
K_M	Krogh's diffusion coefficient in medium

In order to illustrate the application of the nomograms, we are going to determine the O_2 partial pressure at a depth of 100 μm into the above sample spheroid (diameter 500 μm, diameter of central necrosis 100 μm, thickness of diffusion depleted zone 50 μm, $Q=4 \cdot 10^{-4}$ ml O_2/(cm^3 tissue · s), $K_S/K_M=0.5$) for an O_2 partial pressure in the bulk medium of 140 mmHg. First, we calculate the dimensionless coordinates $n'=0.2$, $r'=0.6$, and $g'=1.2$. We conclude that we have to use the marked curve in Fig. 2c. Next, we read the values of the dimensionless

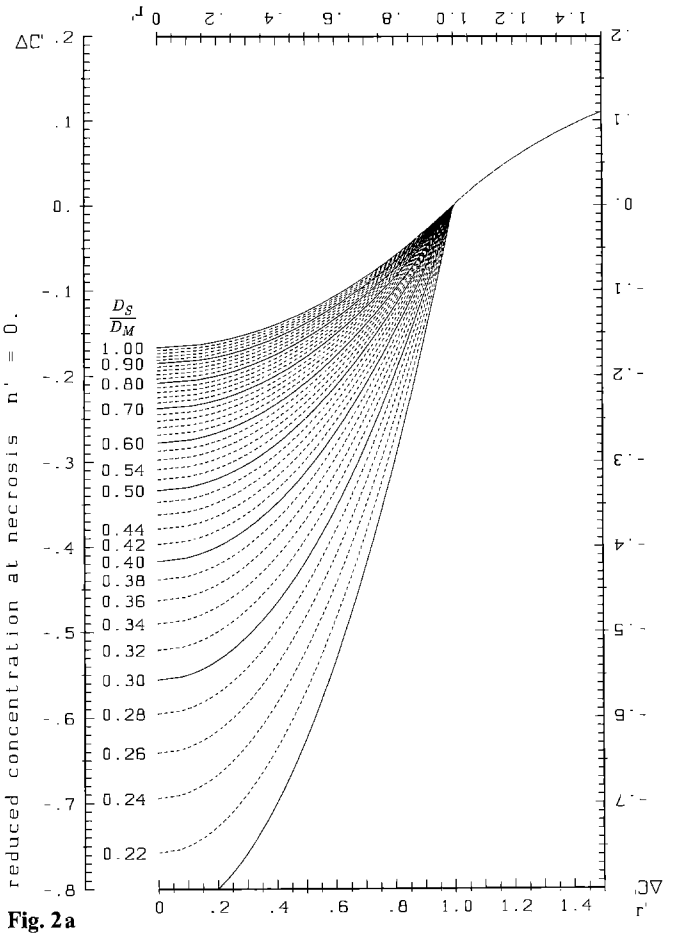

Fig. 2a

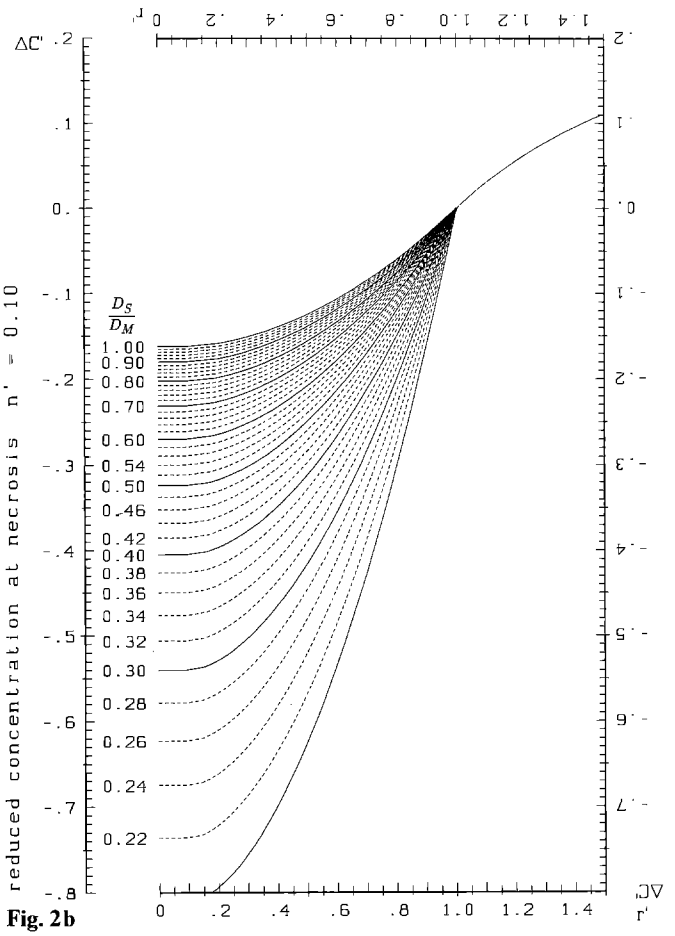

Fig. 2b

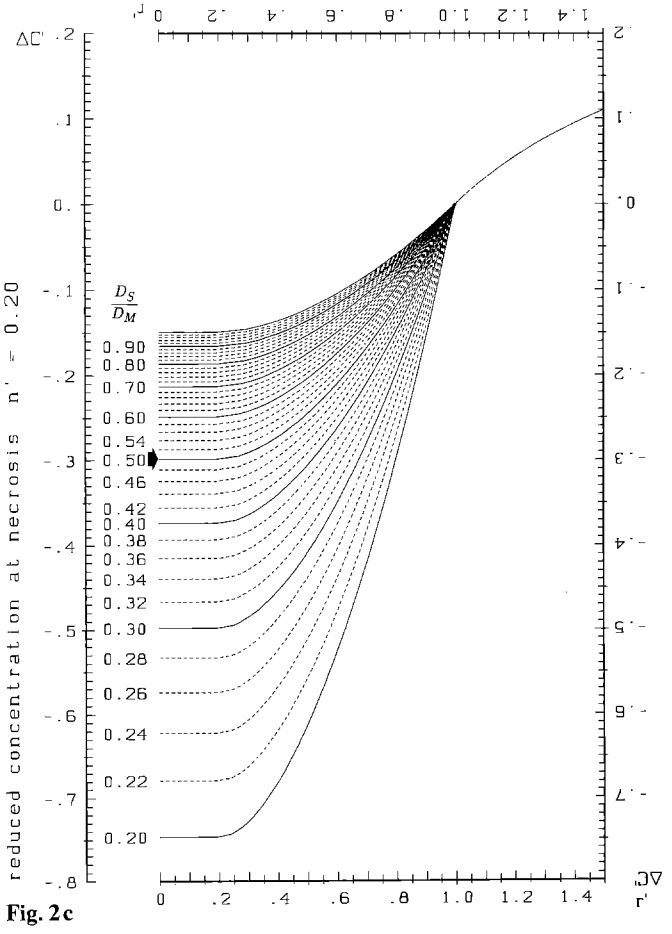

Fig. 2c

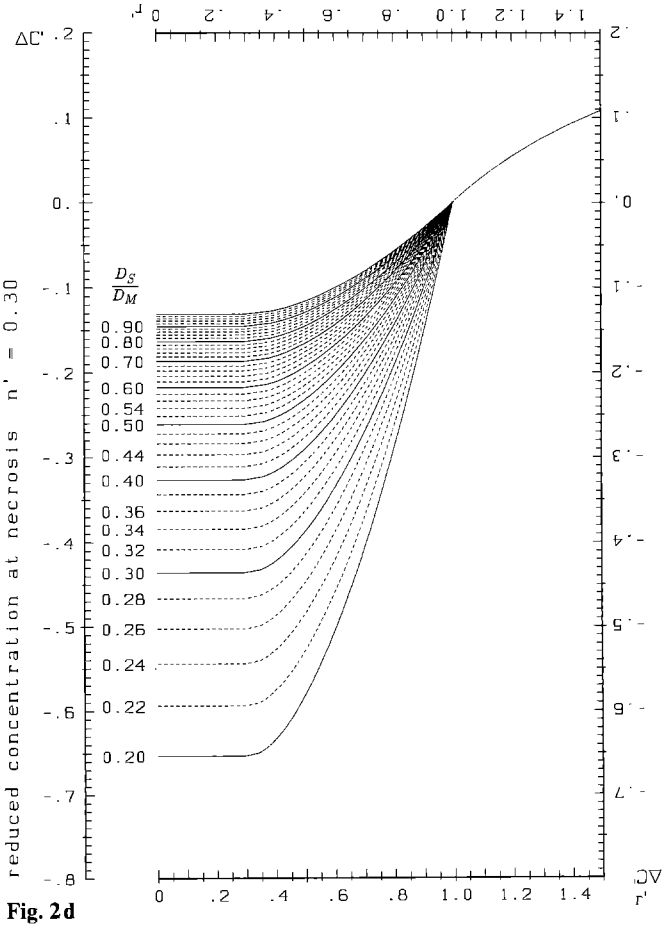

Fig. 2d

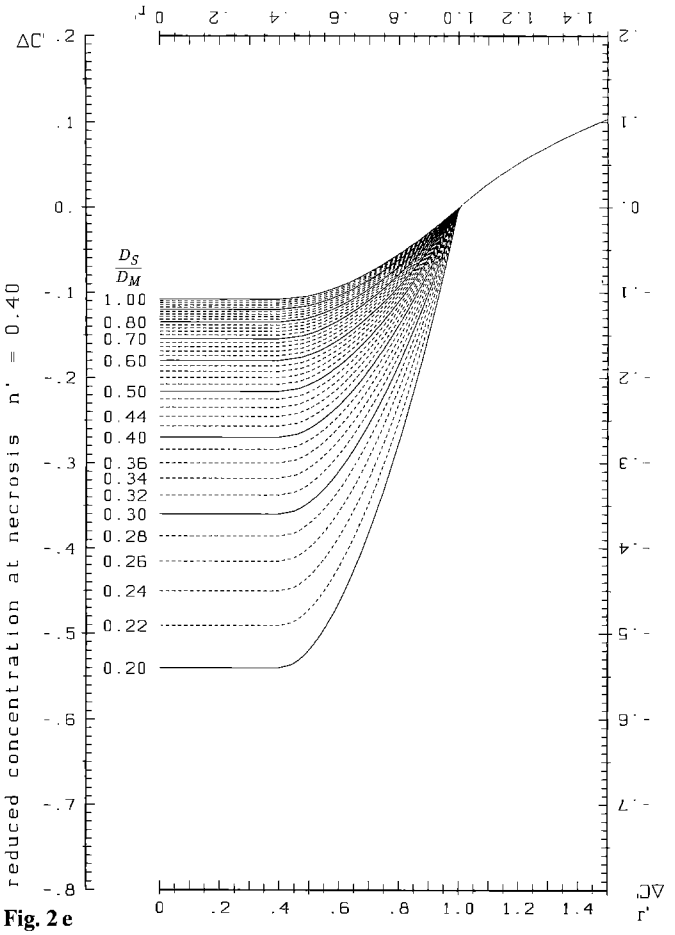

Fig. 2e

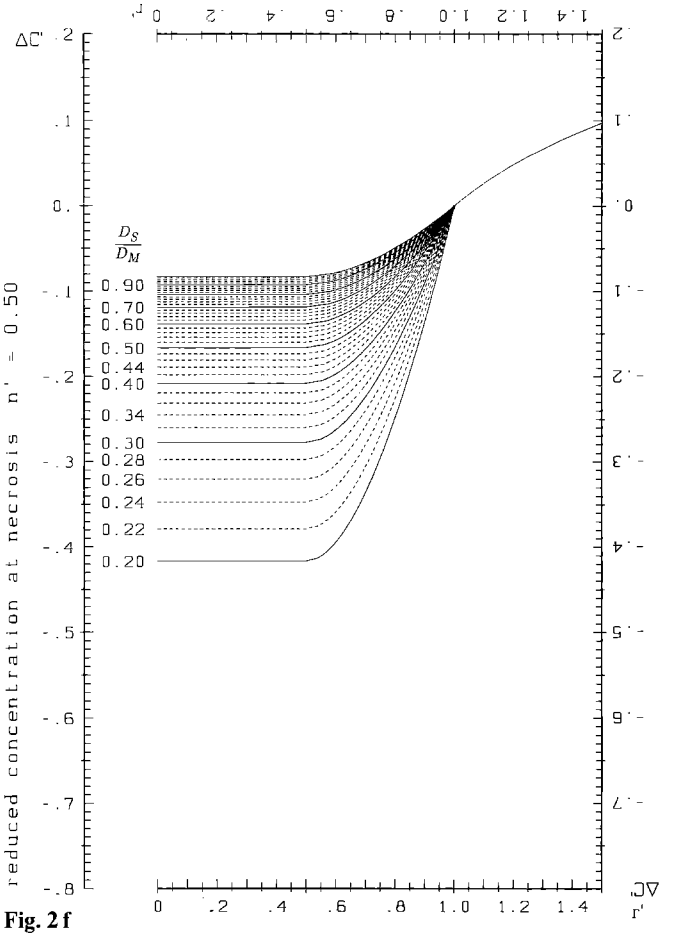

Fig. 2f

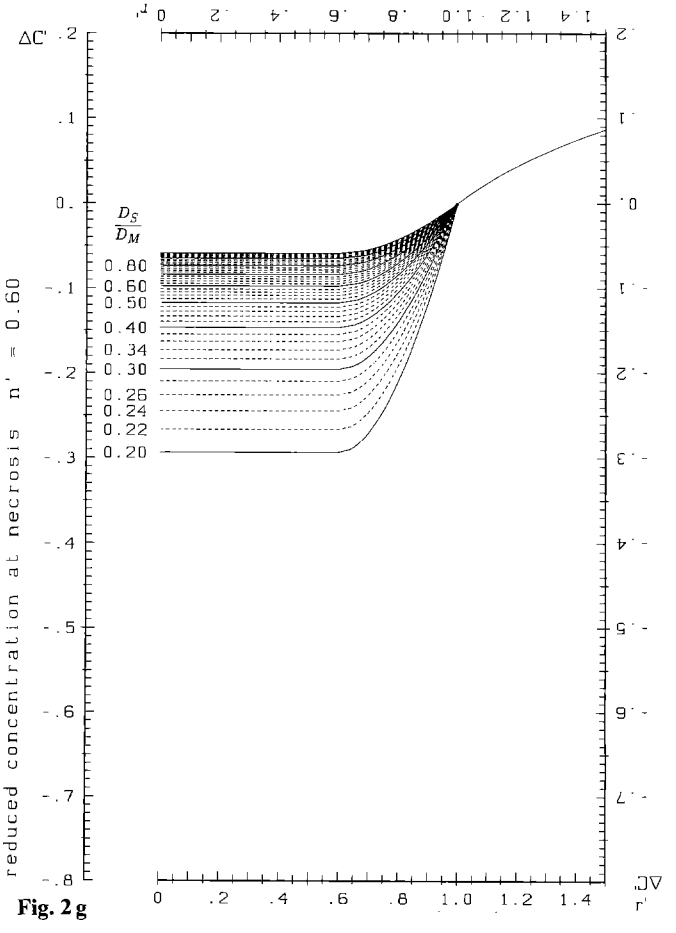

Fig. 2g

Fig. 2a–g. Dimensionless substrate concentration C' (see Eq. (A6)) as a function of dimensionless radial coordinate r' (see Eq. (1)). Diameter of central necrosis equals **a** 0% (no necrosis), **b** 10%, **c** 20%, **d** 30%, **e** 40%, **f** 50%, **g** 60% of the spheroid diameter. The values for C' as read from the nomograms can be transformed to dimensional concentrations C or partial pressures P by means of Eq. (2) or (3), respectively. Each set of curves is parameterized by the ratio of substrate diffusion coefficients in the spheroid and in the medium, D_S/D_M. The concentration of substances which are produced within the spheroid may be obtained by using the upside down scales of the nomograms

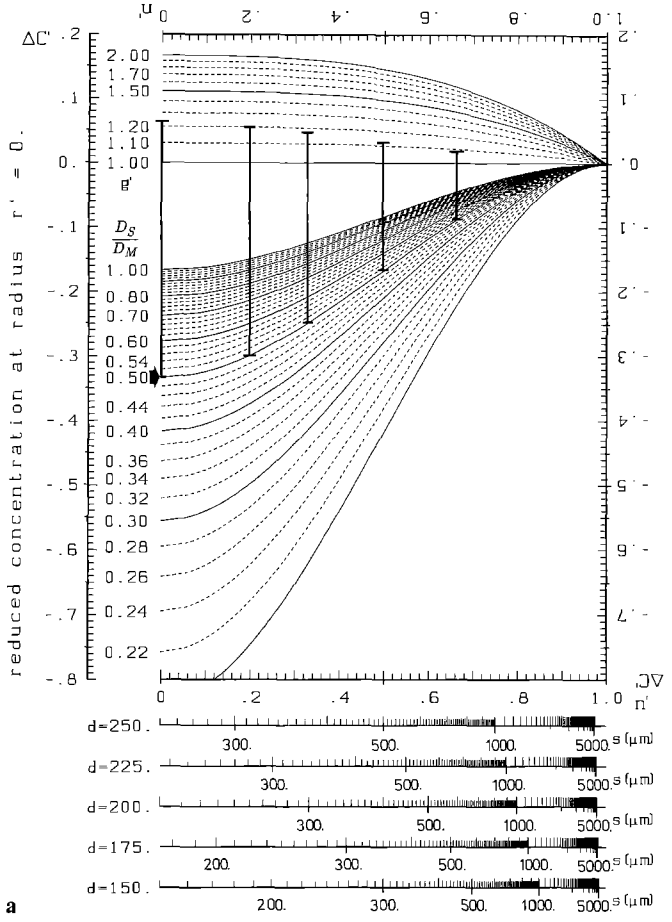

a

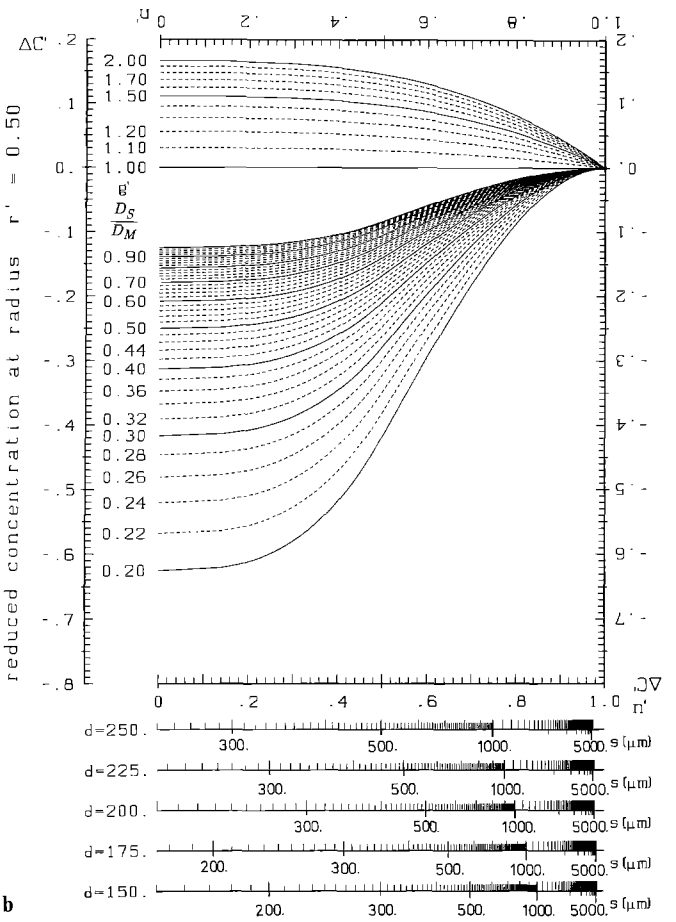

b

Fig. 3a, b. Dimensionless substrate concentration C' at **a** spheroid center and **b** half way into the spheroid as a function of dimensionless radius of central necrosis n'. The additional abscissae display the corresponding spheroid radii s for viable rim thicknesses d given at the left of each scale. In each panel, the two sets of curves describing the contributions of the diffusion depleted zone and of the viable rim towards the concentration of interest are parameterized by the dimensionless radius g' of the diffusion depleted zone (upper set) and by the ratio D_S/D_M of substrate diffusion coefficients in the medium and in the spheroid (lower set), respectively. Dashed vertical lines correspond to central Po_2 values at different stages of spheroid growth (see text)

concentrations at the edge of the diffusion-depleted zone (abscissa $= g' = 1.2$) and at $r' = 0.6$ being 0.058 and -0.210, respectively. Finally, employing (3) (with s given in cm!) we find the desired partial pressure $P = 74.3$ mmHg.

Since the solution of the differential equation of diffusion (A3) is valid independently of the sign of Q, it is possible to apply the nomograms obtained to substances which are produced instead of consumed by the tumor cells, such as lactate. In this case Q is the volume-related production rate and has a negative sign ("negative consumption"). As a consequence, the nomograms have to be used *upside down* with the ordinates given at the right hand side. In the back transformation for the dimensional concentration C (Eq. (2)) or for the partial pressure P (Eq. (3)), a negative Q has to be inserted, so in effect, the second terms of the right hand sides of (2) and (3) change signs.

As an example, we determine the lactate concentration inside a spheroid. On the basis of previous measurements in tumors (Gullino et al. 1967; Swabb et al. 1974), a lactate production rate of $9.64 \cdot 10^{-8}$ mol/(cm^3 tissue · s), a lactate diffusion coefficient of $1.2 \cdot 10^{-5}$ cm^2 s^{-1} in the medium and of $3.5 \cdot 10^{-6}$ cm^2 s^{-1} in the spheroid, a lactate free medium, i.e. $C_B = 0$ mol/cm^3 medium, and the same spheroid geometry as above are assumed. Consequently, we have to use the same diagram and the same abscissae as before but this time with the curve for $D_S/D_M = 3.5 \cdot 10^{-6}/1.2 \cdot 10^{-5} = 0.29$. The dimensionless concentrations read from the nomogram are 0.058 and -0.361. Application of (2) with the appropriately modified sign yields a lactate concentration of $2.10 \cdot 10^{-6}$ mol/(cm^3 tissue) = 18.6 mg/(100 ml tissue), at a depth of 100 μm into the spheroid.

3. Concentrations at fixed dimensionless radii in the growing spheroid

On many occasions, the changes of concentration distributions with spheroid growth are of particular interest. Since the dimensionless size of the central necrosis (= dimensional size over spheroid diameter) changes considerably during spheroid growth, we would have to employ the whole series of diagrams (Fig. 2a–g) to determine the time course of the concentration at one single dimensionless radius r', which is a lengthy and tedious procedure. This may be circumvented by introducing another set of nomograms in which the respective roles of r'

and n' (the dimensionless radius of the necrosis) in the graphs of Fig. 2a–g as abscissal and parameter values have been changed. Two nomograms for dimensionless concentrations as functions of the dimensionless radius of the central necrosis n' at radial positions $r'=0$ (=central concentration) and $r'=0.5$ (half way into the spheroid) are displayed in Fig. 3a, b. Each nomogram is parameterized by D_S/D_M (lower set of curves) and, in addition, by the dimensionless radius of the unstirred layer g' (upper set of curves). During spheroid growth, the viable rim is typically of fairly constant thickness. For a constant viable rim thickness it is possible to use the spheroid radius s in place of n' as abscissa. Five additional abscissal scales of spheroid radii are given, pertinent to viable rim thicknesses d of 150 μm, 175 μm, 200 μm, 225 μm, or 250 μm, respectively. These scales relate the values of n' to the corresponding spheroid radii for the respective viable rim thicknesses. The drop in dimensionless concentration between the bulk medium and the radial position $r'=0$ or $r'=0.5$ may then be found to be the difference between the ordinate values of the appropriate curves from the upper and lower sets. Note that the dimensionless surface concentration ($r'=1$) may be obtained by using only the upper set of curves together with the horizontal line $C'=0$ in the way just described. This way of representation closely approximates the experimental situation, because at least some types of growing spheroids exhibit a rather constant viable rim thickness of 150–250 μm and an accordingly increasing diameter of the central necrosis depending on the cell line and the growth conditions used (Mueller-Klieser and Sutherland 1982a, b; Mueller-Klieser et al. 1986).

Again, we want to illustrate the use of the diagrams by an example (see Table 3). Suppose, we are observing the above sample spheroid growing at a constant viable rim thickness of 200 μm and with a diffusion depleted zone of constant thickness of 50 μm. Suppose, furthermore, that we are interested in the central Po_2 at growth stages characterized by spheroid radii of 200 μm, 250 μm, 300 μm, 400 μm, and 550 μm (line 1 of Table 3). We have to apply Fig. 3a, choosing the abscissal radii from the scale for $d=200$ μm. The dimensionless concentration drops (broken vertical lines in Fig. 3a and line 5 of Table 3) are the differences between the ordinate values of the curves corresponding to the respective g' values (lines 2 and 3 of Table 3) and the curve appertaining to a value of $D_S/D_M=0.5$ (line 4 of Table 3). Applying Eq. (3) with the same constants as above yields the central Po_2 values desired (line 6 of Table 3).

Note from Table 3, that the central Po_2 decreases drastically with increasing spheroid size at constant viable rim and diffusion depleted zone thicknesses. This is in accordance with experimental data obtained in several types of mutlicellular spheroids at different stages of growth (Carlsson et al. 1979; Mueller-Klieser and Sutherland 1982a, b; Carlsson and Acker 1985). At $s=550$ μm, the calculated Po_2 becomes negative, which is not feasible physiologically. We conclude that some of the assumptions made do not hold true any more for spheroids of such a size. The most obvious possibility would be that for the underlying set of parameter values spheroids of this size must exhibit a larger central necrosis due to lack of oxygen. Another explanation could be a decreasing O_2 consumption rate within the viable rim.

Alternatively, one can use Fig. 3a to find the largest viable rim thickness which, at a given spheroid size, can be sufficiently supplied with oxygen. From Eq. (3) (using $P(r)=0$) we find for a 600 μm spheroid that the drop in dimensionless concentration must not exceed 0.099. Figure 3a shows that this value corresponds to a n' of about 0.68. Thus, n must be not be smaller than 408 μm or the viable rim cannot be thicker than 192 μm.

It ought to be mentioned, however, that in several series of experiments the central Po_2 in spheroids showed the predicted decrease with increasing diameter in the lower size range, yet it appeared to slightly increase again as the spheroids attained very large diameters (Mueller-Klieser and Sutherland 1982a; Acker et al. 1984; Freyer et al. 1984; Carlsson and Acker 1985). These observations imply that parameters other than s also vary during spheroid growth. The analysis of measured Po_2 profiles as well as histological investigations are indicative of a decrease in the thickness of the viable rim and of the O_2 consumption rate Q with increasing spheroid size (Mueller-Klieser and Sutherland 1982a, b; Acker et al. 1984; Freyer et al. 1984; Freyer and Sutherland 1985; Tannock and Kopelyan 1986).

4. *Sensitivity analysis*

In Sects. 2 and 3 a formalism is provided which allows one to find the substance concentration at a specified position in a spheroid of known geometry and substance diffusivity and consumption rate. In practice, only aproximations to the numeric values of these parameters characterizing the spheroid of interest are often known. This raises the question of what errors have to be expected in the concentrations obtained from the nomograms. An approximate answer to this question may be given by the following first order sensitivity analysis.

The dependency of the concentration $C(r)$ at radial position r on the parameters defining the spheroid is implicitly contained in (A3) in the Appendix. These parameters (and r) may be combined to form the "parameter vector" $\boldsymbol{p}=(p_i)=(r; n, s, g, Q, D_S, D_M, C_B)$. If we want to emphasize the dependence of C on all its parameters, we are going to write $C(\boldsymbol{p})$ or $C(r; n, s, g, Q, D_S, D_M, C_B)$ instead of $C(r)$. Let $\Delta\boldsymbol{p}=(\Delta p_i)$ denote the "error vector" corresponding to the parameter vector $\boldsymbol{p}$ which is made up of the expected errors in the respective components of $\boldsymbol{p}$. To a first order approximation the error ΔC propagated into C is

$$\Delta C := C(\boldsymbol{p}+\Delta\boldsymbol{p})-C(\boldsymbol{p}) \approx \nabla C(\boldsymbol{p})\cdot\Delta\boldsymbol{p} = \sum_i \frac{\partial C(\boldsymbol{p})}{\partial p_i}\cdot\Delta p_i = \sum_i \frac{\partial C(\boldsymbol{p})}{\partial p_i}\cdot p_i\cdot\frac{\Delta p_i}{p_i} \tag{4}$$

where ∇ is the gradient operator. The derivatives of C with respect to r and the parameters n, s, g, Q, D_S, D_M, and C_B may be calculated from (A3).

Equation (4) shows that the error introduced into $C(\boldsymbol{p})$ at a specific parameter vector $\boldsymbol{p}$ by some fractional

Table 2. Po_2 profile and "sensitivities" evaluated from Table 1 for a "sample spheroid" (see legend of Fig. 1) at different radii. The figures give the local deviation of the calculated Po_2 profile in mmHg corresponding to a 1% error in the respective parameter (i.e. $\Delta p_i/p_i = 0.01$)

	Medium 300	Concentric zones and radial coordinate (μm)						Necrosis 50
		Diffusion depleted zone		Viable rim				
		300	250	250	200	150	100	
Po_2 (mmHg)	140	140	126.5	126.5	97.4	75.1	59.8	53.3
$\frac{\partial Po_2}{\partial r}\frac{r}{100}$ (mmHg)	0	0.675	0.810	1.621	1.029	0.566	0.229	0
$\frac{\partial Po_2}{\partial n}\frac{n}{100}$ (mmHg)	0	0	0.003	0.003	0.013	0.029	0.062	0.160
$\frac{\partial Po_2}{\partial s}\frac{s}{100}$ (mmHg)	0	0	−0.408	−1.219	−1.219	−1.219	−1.219	−1.219
$\frac{\partial Po_2}{\partial g}\frac{g}{100}$ (mmHg)	0	−0.675	−0.675	−0.675	−0.675	−0.675	−0.675	−0.675
$\frac{\partial Po_2}{\partial Q}\frac{Q}{100}$ (mmHg)	0	0	−0.135	−0.135	−0.426	−0.649	−0.802	−0.867
$\frac{\partial Po_2}{\partial D_M}\frac{D_M}{100}$ (mmHg)	0	0	0.135	0.135	0.135	0.135	0.135	0.135
$\frac{\partial Po_2}{\partial D_S}\frac{D_S}{100}$ (mmHg)	0	0	0	0	0.291	−0.514	−0.667	−0.732
$\frac{\partial Po_2}{\partial P_B}\frac{P_B}{100}$ (mmHg)	1.400	1.400	1.400	1.400	1.400	1.400	1.400	1.400

Table 3. Central Po_2 of various spheroid sizes determined from the nomogram in Fig. 3. Po_2 is calculated from C' by means of (3). Except for the spheroid radius s, the underlying data are the same as assumed for the "sample spheroid" (see legend of Fig. 1)

Spheroid radius s (μm)	200	250	300	400	550
g'	1.25	1.20	1.17	1.12	1.09
$C'(s; g')$	0.065	0.053	0.047	0.032	0.020
$C'(s; D_S/D_M = 0.5)$	−0.334	−0.298	−0.247	−0.167	−0.100
$\Delta C'(s)$	0.399	0.351	0.294	0.199	0.120
Central Po_2 (mmHg)	77.4	54.0	36.2	15.1	−2.4

error in the i-th parameter $\Delta p_i/p_i$ may be estimated to be linearly dependent on $\Delta p_i/p_i$ with the "sensitivity" $(\partial C(\boldsymbol{p})/\partial p_i) \cdot p_i$. Table 1 lists these "sensitivities".

Evaluation of the equations in Table 1 for the special case of oxygen diffusing into the above sample spheroid and for a few values of the radial coordinate r yields the numerical sensitivity values compiled in Table 2. Each column of Table 2 lists the Po_2 and the error propagated into Po_2 by a 1% error in the respective parameter indicated in the leftmost column. Propagated errors for other percentages of parameter deviations may be estimated by multiplying the tabulated values by these percentages. To illustrate its use, assume that the expected error in the measured spheroid radius s is ± 25 μm or $\pm 10\%$ of s. Then the error propagated into calculated Po_2 in all of the spheroid would be $-1.22 \cdot (\pm 10)$ mmHg $= \mp 12.2$ mmHg. On the other hand, the same relative error of $\pm 10\%$ in the radius of the central necrosis would introduce an error in calculated Po_2 of ± 0.03 mmHg at the spheroid surface and of ± 1.6 mmHg inside the necrosis. Thus, calculated Po_2 profiles depend much more critically on measurement errors in spheroid radius than in necrosis radius. Table 1 and Eq. (4) may be used to calculate composite errors and errors for different spheroid geometries and substrates.

General discussion

The present approach assumes constant substance consumption/production rates and diffusivities throughout the viable rim of tumor spheroids. Analysis of measured Po_2 profiles has shown that this is a realistic assumption at least for EMT6 spheroids grown under various environmental conditions (Mueller-Klieser et al. 1986). This finding made it possible to describe the entire spheroid system by seven parameters that are most essential for the calculation of substrate concentrations in tumor cell aggregates. If one wanted to display all these dependencies by plotting the respective concentration profiles and wanted to consider, e.g., only five different values of each parameter, one consequently would have to draw $5^7 = 78\,125$ curves. To arrange them with adequate clarity would require at least $5^5 = 3125$ individual diagrams, which would be far beyond the scope of an original paper. Despite this situation, the results obtained demonstrate that – under the above simplifying assumption – a comprehensive mathematical and graphical description of oxygen and substrate distributions in tumor spheroids may be performed by using appropriate coordinate transformations.

The resulting equations or nomograms may also be used for analyzing the concentration profiles of substances that are produced within the cell aggregates, such as lactate.

It has to be kept in mind that consumption and production rates may be functions of the concentrations of related substances, such as oxygen concentration influencing glucose consumption and, hence, lactate production. Depending on the extent of such interrelations, the precision of concentration profiles predicted by the present nomograms may be limited. On the other hand, future application of the analysis developed here to concentration distributions measured may be useful for investigating local variations in consumption/production rates in spheroids.

Also, it should be pointed out that average consumption rates in spheroids are dependent on spheroid size (Freyer and Sutherland 1985; Mueller-Klieser et al. 1986). This has to be taken into account, e.g., when determining substrate concentrations in the center of spheroids as a function of spheroid size. Such an analysis may be biologically relevant, since predictions can be made of the growth stage at which the center of spheroids will eventually become hypoxic. If, in contrast, substance concentrations in the center of growing spheroids have been measured, Fig. 3a and Eqs. (3) and (4) may be used to determine the time course of average substance consumption/production rates in the viable rim during growth.

Previous experimental and theoretical investigations have failed to show a depletion of a single substrate or a toxic concentration of a single waste product as a cause of cell death in spheroids (Mueller-Klieser and Sutherland 1982a, b; Mueller-Klieser et al. 1986). This is another field in which the present approach may be useful. Statistical analysis of various combinations of substrate concentrations obtained from the procedure suggested may reveal biological mechanisms which contribute to the development of necrosis. Furthermore, the extent of changes in substrate concentrations upon manipulation of inhibitors of the cellular respiratory activity, may be predicted on the basis of the present nomograms. Finally, the framework presented allows for a parameter sensitivity analysis with regard to the determination of consumption rates Q and diffusion constants D_S, from measured concentration distributions by regression analysis which will be subject to further investigations.

Acknowledgement. This study was supported by the Deutsche Forschungsgemeinschaft (Mu 576/2-3, Mu 576/2-4).

Appendix

In order to calculate the concentration C of a metabolically active substance at a given time t and a given location inside a multicellular tumor spheroid the differential equation of simultaneous substrate diffusion and consumption/production has to be solved. The general form of this equation may be written as

$$\frac{\partial C}{\partial t} = \nabla(D\,\nabla C) - Q \tag{A1}$$

where ∇ is the gradient operator D is the diffusion coefficient or diffusivity and Q is the substance consumption/production rate. In the case of a gaseous substrate, the driving forces for diffusion are partial pressure gradients, not concentration gradients. Therefore the concentration C has to be replaced by the partial pressure P and Q has to be divided by the (local) solubility.

Analytic solutions have been obtained for a number of special cases and for a variety of boundary conditions (for reviews see: Grossmann et al. 1984; Mueller-Klieser 1984a; Freyer and Sutherland 1986). In the special case of tumor spheroids, the diffusion geometry is assumed to exhibit spherical symmetry – i.e. the concentration distribution depends solely upon the radial coordinate r – making a transformation to polar coordinates advantageous. The present study is to describe spheroids under steady state conditions, i.e., D, Q, and the boundary conditions are constant with time. Thus, $\partial C/\partial t$ vanishes, and (A1) may be transformed to yield

$$D\left(\frac{d^2C}{dr^2} + \frac{2}{r}\frac{dC}{dr}\right) - Q = 0 \tag{A2}$$

Equation (A2) is to be solved for multicellular spheroids cultured in stirred media. Previous investigations have shown that at a certain stage of growth, these spheroids develop a central necrotic region, surrounded by a rim of viable cells. Furthermore, the cell aggregates exhibit a diffusion depleted layer of unstirred medium at their surface (Mueller-Klieser and Sutherland 1982a). Taking into account appropriate boundary and interface conditions, Eq. (A2) was solved by Mueller-Klieser (1984a) for these different regions resulting in a set of equations, a slight modification of which is given below:

$$C(r) = \begin{cases} C_B & r > g \\ C_B - \dfrac{Q}{3D_M}(s^3 - n^3)\left(\dfrac{1}{r} - \dfrac{1}{g}\right) & s < r \le g \\ \left.\begin{aligned} &C_B - \frac{Q}{3D_M}(s^3 - n^3)\left(\frac{1}{s} - \frac{1}{g}\right) \\ &\quad - \frac{Q}{6D_S}\left(s^2 - r^2 + \frac{2n^3}{s} - \frac{2n^3}{r}\right) \end{aligned}\right\} & n < r \le s \\ \left.\begin{aligned} &C_B - \frac{Q}{3D_M}(s^3 - n^3)\left(\frac{1}{s} - \frac{1}{g}\right) \\ &\quad - \frac{Q}{6D_S}\left(s^2 + \frac{2n^3}{s} - 3n^2\right) \end{aligned}\right\} & r \le n \end{cases} \tag{A3}$$

where the following notations are used:

D_M, D_S	diffusion coefficients in the medium and in the spheroid, respectively
Q	volume-related substrate consumption/production rate (negative in the case of production)
n, s, g	radii of central necrosis, spheroid, and diffusion-depleted zone, respectively
C_B	substance concentration at the interface between stirred medium and diffusion-depleted zone

If there is emphasis on the dependence of C on not only r but also the parameters defining the "spheroid system" we use the notation $C(r; n, s, g, Q, D_S, D_M, C_B)$.

Determination of D_S/D_M from the slopes at the spheroid surface

From Eqs. (A3) the slopes of $C(r)$, dC/dr, may be directly calculated. Let $dC/dr(s^+)$ and $dC/dr(s^-)$ denote the limits of dC/dr, if r approaches s from above or from below, respectively. Then we have

$$\frac{\frac{dC}{dr}(s^+)}{\frac{dC}{dr}(s^-)} = \frac{\lim\limits_{r \searrow s} -\frac{Q}{3D_M}\left(-\frac{1}{r^2}\right)(s^3-n^3)}{\lim\limits_{r \nearrow s} -\frac{Q}{6D_S}\left(-2r+\frac{2n^3}{r^2}\right)} = \frac{D_S}{D_M}. \tag{A4}$$

Description of concentration distributions in tumor cell aggregates by dimensionless coordinates

We now define the dimensionless radial coordinate r'.

$$r' = \frac{r}{s}; \text{ and accordingly } n' = \frac{n}{s}; \; g' = \frac{g}{s}.$$

Substituting this into Eqs. (A3) and substracting C_B from either side yields:

$$C(r)-C_B = \begin{cases} 0 & r' > g' \\ -\frac{Q}{3D_M} s^3 (1-n'^3) \frac{1}{s}\left(\frac{1}{r'}-\frac{1}{g'}\right) & 1 < r' \le g' \\ \left.\begin{aligned} &-\frac{Q}{3D_M} s^3 (1-n'^3) \frac{1}{s}\left(1-\frac{1}{g'}\right) \\ &-\frac{Q}{6D_S} s^2 \left(1-r'^2+2n'^3-\frac{2n'^3}{r'}\right) \end{aligned}\right\} & n' < r' \le 1 \\ \left.\begin{aligned} &-\frac{Q}{3D_M} s^3 (1-n'^3) \frac{1}{s}\left(1-\frac{1}{g'}\right) \\ &-\frac{Q}{6D_S} s^2 (1+2n'^3-3n'^2) \end{aligned}\right\} & r' \le n' \end{cases} \tag{A5}$$

From Eqs. (A5) it is obvious that there is a linear dependence of $C(r)-C_B$ on the consumption/production rate Q and the spheroid surface $4\pi s^2$, which may be eliminated from the right hand sides of (A5) by division of both sides by $Q \cdot s^2$. Multiplication of either side by D_M reduces the dependence on both diffusion coefficients D_M and D_S to the dependence on the ratio D_M/D_S alone. By rearrangement of (A5), the number of independent variables present in the right hand sides is minimized. Defining the left hand side to be the dimensionless concentration C':

$$C'(r') = \frac{D_M(C(r' \cdot s)-C_B)}{Q \cdot s^2} \tag{A6}$$

we have the transformed set of (A7):

$$C'(r') = \begin{cases} 0 & r' > g' \\ \left(1-\frac{1}{r'}\right)\frac{1-n'^3}{3} & 1 < r' \le g' \\ -\frac{D_M}{6D_S}\left(1-r'^2-2n'^3\left(\frac{1}{r'}-1\right)\right) & n' < r' \le 1 \\ -\frac{D_M}{6D_S}(1+2n'^3-3n'^2) & r' \le n' \end{cases} - \left(1-\frac{1}{g'}\right)\frac{(1-n'^3}{3} \tag{A7}$$

The dependence of C' upon the parameters other than r' is restricted to the variables D_M/D_S, g', and n'. In analogy to the above notation, C' may therefore be written as $C'(r'; n', g', D_M/D_S)$.

From this set of equations the dimensionless concentration profiles in Figs. 2 and 3 have been calculated for different parameter values. To achieve a most convenient application of the diagrams, the origin of the dimensionless concentration scale was positioned to the spheroid surface.

In the case of gaseous solutes, such as oxygen, the very same set of equations and diagrams will apply, if concentrations C and diffusion coefficients D_M, D_S are replaced by partial pressures P and by diffusion conductivities K_M, K_S (Krogh's diffusion constants), respectively.

Table 4. Unstirred layer thickness (in μm) in Bellco spinner flasks (at 190 rpm) for some substrates/waste products and for different spheroid radii

Substrate/waste product	Radius (μm)		
	200	400	600
Oxygen	76	71	68
Glucose	68	63	60
Lactate	70	65	62
Hydrogen ion	86	81	78

Assessment of unstirred layer thickness

Mass transfer coefficients k_m of unstirred layers surrounding spheroids have been determined by Casciari (1989). k_m is defined by

$$\text{substance flux} = 4 \cdot s^2 \cdot k_m \cdot (C_B - C(s)).$$

Using (A3) the substance flux into/out of the spheroid may be calculated and substituted in the definition for k_m, yielding:

$$k_m \cdot s^2 \cdot (s^{-1} - g^{-1}) = D_M .$$

From this equation, the unstirred layer thickness $g - s$ can be calculated as a function of k. Casciari (1989) gives mass transfer coefficients (in terms of Sherwood numbers) for a number of substrates and waste products. In Table 4, corresponding unstirred layer thicknesses are listed for spheroid radii of 200, 400, and 600 μm.

References

Acker H, Carlsson J, Durand RE, Sutherland RM (1984) Spheroids in cancer research: methods and perspectives. Springer, Berlin Heidelberg New York

Bush NA, Bruley DF, Bicher HI (1982) Identification of viable regions in "in vivo" spheroidal tumors: a mathematical investigation. Adv Exp Med Biol 157:1–7

Carlsson J, Acker H (1985) Influence of oxygen pressure in culture medium on the oxygenation of different types of multicellular spheroids. Int J Radiat Oncol Biol Phys 11:535–546

Carlsson J, Acker H (1988) Relations between pH, oxygen partial pressure and growth in cultured cell spheroids. Int J Cancer 42:715–720

Carlsson J, Nederman T (1989) Tumor spheroid technology in cancer therapy research. Eur J Cancer Clin Oncol 25:1127–1133

Carlsson J, Stalnacke CG, Acker H, Haji-Karim M, Nilsson S, Larson B (1979) The influence of oxygen on viability and proliferation in cellular spheroids. Int J Radiat Oncol Biol Phys 5:2011–2020

Casciari JJ (1989) The effects of the diffusion and reaction of nutrients and metabolic waste products on the growth and microenvironment of multicellular tumor spheroids. Ph. D. thesis, University of Rochester, Rochester, NY

Conger AD, Ziskin MC (1983) Growth of mammalian multicellular tumor spheroids. Cancer Res 43:556–560

Freyer JP, Sutherland RM (1983) Determination of diffusion constants for metabolites in multicell tumor spheroids. Adv Exp Med Biol 159:463–465

Freyer JP, Sutherland RM (1985) A reduction in the in site rates of oxygen and glucose consumption of cells in EMT6/Ro spheroids during growth. J Cell Physiol 124:516–524

Freyer JP, Sutherland RM (1986) Regulation of growth saturation and the development of necrosis in multicell spheroids by the oxygen and glucose supply. Cancer Res 46:3504–3512

Freyer JP, Tustanoff E, Franko AJ, Sutherland RM (1984) In situ oxygen consumption rates of cells in V-79 multicellular spheroids during growth. J Cell Physiol 118:53–61

Grossmann U, Winkler P, Carlsson J, Acker H (1984) Local variations of oxygen consumption within multicellular spheroids calculated from measured PO_2-profiles. Adv Exp Med Biol 169:719–728

Gullino PM, Grantham FH, Courtney AH (1967) Glucose consumption by transplanted tumors in vivo. Cancer Res 27:1031–1040

Kawashiro T, Nüsse E, Scheid P (1975) Determination of oxygen and carbon dioxide in respiring tissue: results in rat skeletal muscle. Pflügers Arch 359:231–251

Mueller-Klieser W (1984a) Method for determination of oxygen consumption rates and diffusion coefficients in multicellular spheroids. Biophys J 46:343–348

Mueller-Klieser W (1984b) Microelectrode measurement of oxygen tension distributions in multicellular spheroids cultured in spinner flasks. In: Acker H, Carlsson J, Durand R, Sutherland RM (eds) Spheroids in cancer research: methods and perspectives. Springer Berlin Heidelberg New York, pp 134–149

Mueller-Klieser W (1987) Multicellular spheroids: A review on cellular aggregates in cancer research. J Cancer Res Clin Oncol 113:101–122

Mueller-Klieser W, Sutherland RM (1982a) Influence of convection in the growth medium on oxygen tensions in multicellular tumor spheroids. Cancer Res 42:237–242

Mueller-Klieser W, Sutherland RM (1982b) Oxygen tensions in multicell spheroids of two cell lines. Br J Cancer 45:256–264

Mueller-Klieser W, Freyer JP, Sutherland RM (1986) Influence of glucose and oxygen supply conditions on the oxygenation of multicellular spheroids. Br J Cancer 53:345–353

Sutherland RM (1988) Cell and environment interactions in tumor microregions: The multicell spheroid model. Science 240:117–256

Swabb EA, Wei J, Gullino PM (1974) Diffusion and convection in normal and neoplastic tissues. Cancer Res 34:2814–2822

Tannock IF, Kopelyan I (1986) Influence of glucose concentration on growth and formation of necrosis in spheroids derived from a human bladder cancer cell line. Cancer Res 46:3105–3110